AIAA JOURNAL
Vol. 35, No. 4, April 1997

Using Controlled Unsteady Fluid Mass Addition to Enhance Jet Mixing

Ganesh Raman*
NYMA Inc., Brook Park, Ohio 44142

A rectangular jet was excited by controlled unsteady fluid mass addition using two miniature fluidic jets placed on either side of its narrow dimension. The subharmonic of the primary's preferred jet column frequency [$St(D_e) = fD_e/U_j = 0.15$] was forced in the antisymmetric mode because such forcing persists for longer downstream distances than the fundamental. Details of the phase-averaged flowfield, velocity gradient terms, velocity spectra, and the mean and fluctuating flowfields were documented. The fluidically excited mode grew and persisted in the flow beyond the potential core region. Unsteady fluid mass addition of 12% (4% momentum addition) per fluidic jet resulted in a 35% reduction of the potential core length and about a 60% increase in the normalized mass flux (percentages are with reference to the primary unforced jet). On the basis of the results, it appears that fluidic devices have the potential for use in shear flow control applications.

Nomenclature

A = nozzle exit area of outer flip-flop attachment
A_p = nozzle exit area of primary nozzle
a = nozzle exit area of inner nozzle of flip-flop apparatus
B = larger dimension of outer flip-flop attachment
B_p = larger dimension of primary nozzle
b = larger dimension of inner nozzle of flip-flop apparatus
c = phase velocity, $c = f\lambda = 2\pi f/\alpha_r$
D_e = equivalent diameter of the primary rectangular nozzle
f = frequency of oscillation
H = smaller dimension of outer flip-flop attachment
H_p = smaller dimension of primary nozzle
h = smaller dimension of inner nozzle of flip-flop apparatus
L_{ff} = axial dimension of flip-flop attachment (see Fig. 1)
$\dot{m}$ = mass flux
$\dot{m}_{ff}$ = mass flux at exit of flip-flop nozzle
$\dot{m}_o$ = mass flux at exit of primary nozzle
P_a = ambient pressure
P_o = reservoir pressure
S, S_p, s = aspect ratio, B/H, B_p/H_p, b/h
St = Strouhal number, $St(D_e) = fD_e/U_j$, $St(h) = fh/U_j$
t = time
$U, \bar{u}$ = axial mean velocity
U_{ff} = exit mean velocity at outer nozzle of flip-flop apparatus
U_{iff} = exit mean velocity at inner nozzle of flip-flop apparatus
U_j = exit mean velocity of primary jet
$\langle u \rangle$ = phase-averaged axial velocity, $\langle u \rangle = \bar{u} + \tilde{u}$
$\langle u_f \rangle$ = coherent component of axial velocity at frequency f
$u\prime$ = total fluctuating component of axial velocity, $u\prime = \tilde{u} + \hat{u}$
$\tilde{u}$ = coherent component of axial velocity
$\hat{u}$ = random component of axial velocity
V = transverse mean velocity
$\langle v \rangle$ = phase-averaged transverse velocity
$v\prime$ = total fluctuating component of transverse velocity
w = width of feedback slot (see Fig. 1)
x = axial distance
y = transverse distance
$y_{1/2}$ = half-velocity spread
z = spanwise distance
$\alpha, (\alpha_r)$ = streamwise wavenumber (real)
δ^* = displacement thickness
θ = momentum thickness
λ = wavelength
ω = frequency parameter, $2\pi f$

Received Nov. 16, 1995; revision received Dec. 23, 1996; accepted for publication Jan. 24, 1997.

*Senior Research Engineer, Experimental Fluid Dynamics Section, NASA Lewis Research Center Group. Member AIAA.

I. Introduction

AN experimental investigation of shear flow excitation using controlled unsteady fluid mass addition was conducted. A pair of miniature fluidically oscillated jets that could produce a time-varying flow with a controllable frequency, magnitude, and relative phase (between the two oscillating jets) was used to excite a larger scale "primary" jet flow. The main motivation was provided by the expectation that unsteady fluid mass addition at the right frequency would enhance jet mixing and thus provide a practical means to excite and control shear flow. A rectangular geometry was chosen for the larger scale primary jet because of the presence of a sinuous instability about its smaller dimension further downstream and because of the importance of this nozzle shape in technological applications. Because the goal was to force a sinuous instability, the rectangular jet flow was expected to be more receptive to such forcing. The sinuous mode (antisymmetric in $u\prime$ and symmetric in $v\prime$) was forced by using two miniature fluidic devices on either side of the primary nozzle's narrow dimension. The fluidic devices had no moving parts and were interconnected to provide the desired phase difference. The frequency of the miniature oscillating jets was chosen to match that of the subharmonic of the preferred jet column mode—based on the D_e of the rectangular jet. The subharmonic frequency was chosen because its effect persists over a greater downstream distance than the fundamental.

The fluidic excitation method presented in this paper has the potential to overcome difficulties associated with applying acoustic excitation in practical applications. Although a majority of previous studies on shear layer dynamics and jet mixing control have employed acoustic excitation (e.g., Refs. 1–7), they did so only because acoustic drivers allowed them to produce any frequency or amplitude of a desired pure axisymmetric or azimuthal mode (or combinations) with negligible contamination. Acoustic drivers are thus an invaluable tool for providing insight into shear layer flow physics. However, acoustic drivers are not suitable for controlling flows of practical interest because of their enormous weight, power, and maintenance requirements. In addition, as the Mach number increases and the background noise and turbulence increase, the amplitude of excitation from acoustic drivers would be insufficient

to bring about large changes in the mean flow. It appears that fluidic excitation devices may have the potential to overcome the difficulties mentioned in the preceding.

In recent years, a variety of novel fluid flow control devices have been developed. These include the whistler nozzle,[8] suction at the jet periphery,[9] and the use of piezoelectric actuators.[10,11] In the whistler nozzle,[8] a collar installed downstream of the nozzle exit interacts with the flow to produce an acoustic tone that excites the jet and enhances mixing. Further, the collar dimensions can be tailored to produce a tone that matches the natural frequency of the jet. Suction around the jet periphery[9] causes the jet to transition from a convective to absolute instability. Large mixing rates that result from this technique have been attributed to the presence of the absolute instability. In the piezoelectric excitation technique,[10,11] the actuators are driven with a carrier wave that is amplitude modulated with the desired excitation waveform. In one study,[10] four piezoelectric actuators were phased to excite various modes in a square jet. Note that the present technique is different because unsteady fluid mass is added to the flow. In addition, the present work does not employ an amplitude-modulated waveform. The only similarity between the piezoelectric actuators and the fluidic oscillators is that their relative phases are controllable.

Davis[12] used radial blowing from a pair of steady control jets and obtained variable control of the jet by adjusting the penetration of the control jets into the main jet flow. Berman and Andersen[13] used auxiliary jet injection to control the noise of a jet flow. The main difference between the present work and that in Refs. 12 and 13 is the dynamic control aspect (i.e., instead of steady jets, the present work uses unsteady control jets that are oscillating at a frequency to which the primary jet is unstable).

II. Experimental Details

A. Fluidic Oscillator Nozzles

In a pioneering paper on the "flip-flop jet nozzle," Viets[14] applied fluid control ideas to jet nozzles, showing that it is possible to produce and sustain an oscillating jet flow without any moving parts. In a later paper, Viets[15] described the dynamics of a jet emerging from a fluidic nozzle and its applications. At the NASA Lewis Research Center, a related effort was initiated in 1991 to study fluidic jets[16–18] and to use fluidic oscillator nozzles as excitation devices.[19] The fluidic excitation idea was obtained from Rice and Zaman[20] and also from Brown and Ahuja.[21] Although a brief Note was published on the use of fluidic excitation,[19] details of such flows remain unexplored. A brief description of the fluidic jet nozzle follows.

Figure 1a shows an exploded view of the fluidic jet nozzle. The nozzle shown has three parts: the convergent rectangular slot nozzle with exit dimensions h and b, a nozzle attachment with exit dimensions H and B (Fig. 1b), and a feedback tube that connects the control ports on the nozzle attachment (dimensions are given in Table 1). Flow from the inner nozzle, issuing between the two plates of the nozzle attachment, could attach to either wall because of the Coanda effect. The equalization of pressures provided by the feedback tube causes the jet to detach from one wall and attach to the other. By repetition of this process, an oscillating jet flow is achieved (for operational details, see Ref. 14). An aspect ratio (b/h) of 8 was selected for the inner slot nozzle in this work, because for very small aspect ratios the oscillation stops because of end-wall effects, and for very large aspect ratios there is spanwise nonuniformity in the phase of oscillation.

Key characteristics of fluidic jets are depicted in Fig. 2. Figure 2a indicates that the spectrum of a fluidic exciter device consists of a fundamental frequency and three harmonics. The harmonics are present because of the on–off (square wave) character of the flow coming through this device (see Fig. 2b). Finally, the oscillation frequency vs nozzle pressure ratio is shown in Fig. 2c. Note that the frequency cannot be changed without altering the mass flow through the nozzle. Thus, in using this excitation device, one should be concerned not only with the frequency of excitation but also with the mass of fluid being added.

B. Experimental Techniques

Hot-film probes were used for obtaining flowfield data. The hot-film probes (TSI 1210-20) were used with constant temperature anemometer circuits (Dantec 55M01 and 55M10) and were operated at an overheat ratio of 1.8. A microvax 3300 computer was used for data acquisition and processing. The data acquisition system had eight channels of analog-to-digital converters with a 100-KHz sampling rate and another module with four channels of analog-to-digital conversion with a sampling rate of 1 MHz. The hot-film probes were calibrated in situ at the exit plane of the primary jet by using the velocity determined by the static pressure in the plenum tank. The cosine law assumption was used for the x wires. During

Table 1 Dimensions and experimental conditions[a]

Primary nozzle				
H_p, mm	B_p, mm	$S_p = B_p/H_p$	$A_p = B_p H_p$, mm^2	U_j, m/s
22.36	67.08	3	1500	43.2
Flip-flop (inner nozzle)				
h, mm	b, mm	$s = b/h$	$a = bh$, mm^2	U_{iff}, m/s
2.34	19.05	8.15	44.58	210
Flip-flop (outer attachment)				
H, mm	B, mm	$S = B/H$	$A = BH$, mm^2	U_{ff}, m/s
7.0	19.05	2.72	134	70

[a] All nozzles are rectangular.

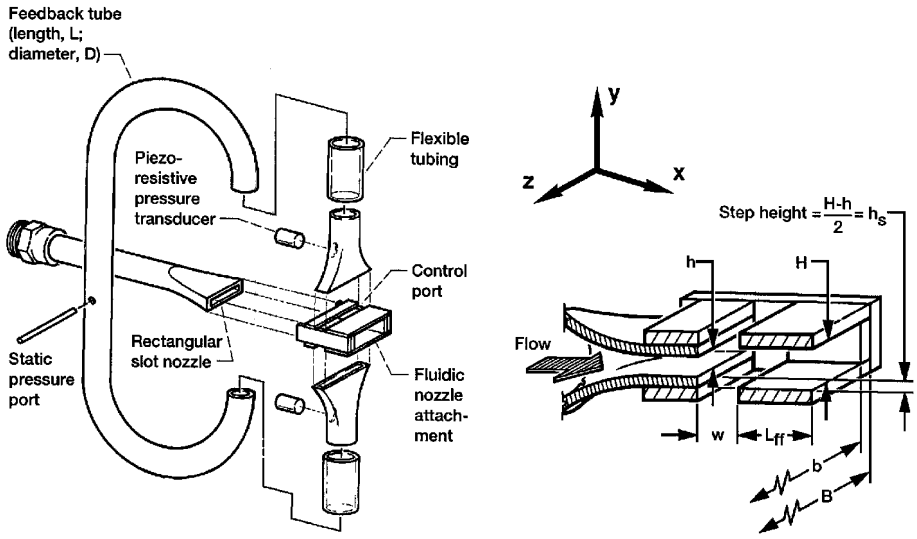

a) Exploded view of fluidic jet nozzle b) Details of fluidic nozzle attachment

Fig. 1 Schematic diagram of a fluidic excitation device.

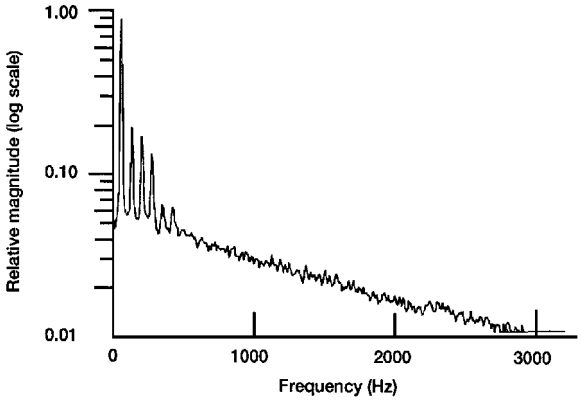

a) Streamwise velocity spectrum

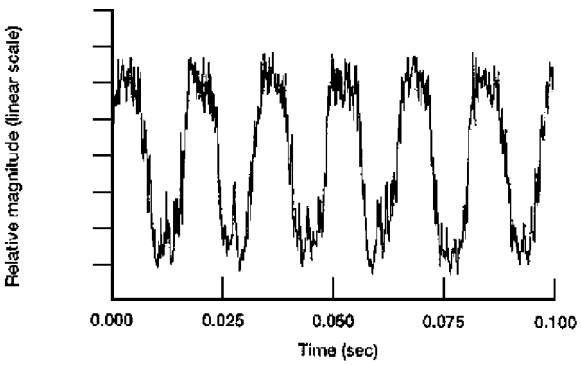

b) Time trace of streamwise velocity

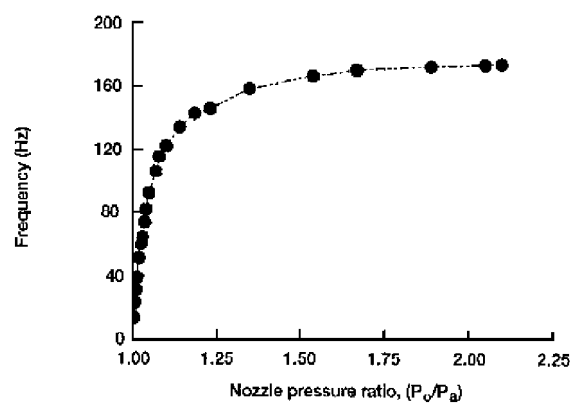

c) Oscillation frequency vs nozzle pressure ratio

Fig. 2 Characteristics of a fluidic excitation device.

this investigation, both methods of linearization were used—i.e., a fourth-order polynomial fit to the calibration data or a linearizer circuit (Dantec 55M25).

For measurement of the oscillating static pressure in the feedback tube, two piezoresistive pressure transducers mounted on either end of the feedback tube were used. A vacuum pump was used for static calibration of these transducers to measure subatmospheric pressures (0–105 KPa). A pressure port in the feedback tube was used to measure the mean static pressure. Smoke flow visualization was accomplished by filling the plenum chamber with smoke and illuminating the flowfield with bright continuous light (750 W). The smoke was produced by electrically igniting smoke candles in a pressurized chamber. The smoke candles used were available commercially for use as emergency signaling devices and for producing theatrical effects. The smoke generated by this means fed the fluidic jet. A camera that could freeze images to 0.0001 s captured the images.

C. Data Reduction Techniques

In addition to obtaining mean flow parameters (such as U, V) and averaged rms quantities (such as $u\prime$, $v\prime$), phase-averaged realizations of the flow were obtained. The triple decomposition, which is now quite common in periodic turbulent flows, was applied. In this case, the decomposition for u would be $u = \bar{u} + \tilde{u} + \hat{u}$, where $\bar{u}$ is the mean value, $\tilde{u}$ is the coherent periodic fluctuation, and $\hat{u}$ is the random turbulence fluctuation. By phase averaging, we measure $\langle u \rangle = \bar{u} + \tilde{u}$ (note that $\langle \hat{u} \rangle = 0$).

Phase-averaged velocity measurements of the entire flowfield of the fluidic exciter jet as well as the primary flow excited by the fluidic jets were made. For these measurements, a reference hot-film probe (for the trigger signal) was located near the exit of the fluidic exciter jet. The reference probe was displaced in z by 2 mm with respect to the measurement probe to avoid wake interference effects. The measurement probe that was mounted on the three-dimensional traversing system moved over the entire flowfield. Phase-averaged measurements were ensemble-averaged over 100 oscillation cycles. The data acquisition rate was chosen so that the phase-averaged distributions could be computed for 40 time steps per cycle. The data acquisition rate for the fluidic jet alone was 2 KHz, whereas the data acquisition rate for the primary jet excited by the fluidic oscillators was 5 KHz. For the phase-averaged data acquired over the entire XY plane the Δx and Δy were 12.7 and 2.54 mm for the fluidic jet and 12.7 and 5.08 mm for the primary jet excited by the fluidic jets. The phase-averaged velocity components (axial, $\langle u \rangle$; transverse, $\langle v \rangle$) were measured over the entire xy plane with an x-film probe. Phase averaging allowed observation of the instantaneous motions occurring during one cycle of oscillation.

D. Experimental Uncertainty and Sources of Errors

Measurement uncertainty certainly did influence the results. The largest uncertainties were in the region where the flow from the exciter jets merged with the primary jet flow. For the phase-averaged x-film and single-film measurements, data were taken downstream of this merging region, which avoided the measurement difficulties in the merging region. Estimates for the measurement uncertainty were obtained by the methods described by Moffatt.[22] For the hot-film probes, the calibration uncertainty for $u/u_j > 0.4$ was 1%, and the first-order uncertainty was $< 0.5\%$, yielding a total uncertainty of 1.12%. However, when the probe was placed near the exit of the fluidic nozzle ($x/h < 5$), or near the edge of the jet, the errors were much larger ($\sim$10%) because the larger flow angularities invalidated the Cosine law used for the x-wire calibration. For the piezoresistive pressure transducers, the calibration uncertainty was 1.5%, and the first-order uncertainty was 0.3%, yielding a total uncertainty of 1.53%. The uncertainty was 1 Hz in the frequency measurements and $\pm$5 deg in the phase measurement.

III. Flowfield of Fluidic Jets

Smoke flow visualization photographs of the fluidic jet oscillation (reproduced from Ref. 18) are shown in Fig. 3. The photographs vividly illustrate the two phases of oscillation. The $\langle u \rangle$ distributions for a fluidically oscillated jet operated at 70 m/s are shown in Fig. 4. Although the phase-averaged distributions were computed for 40

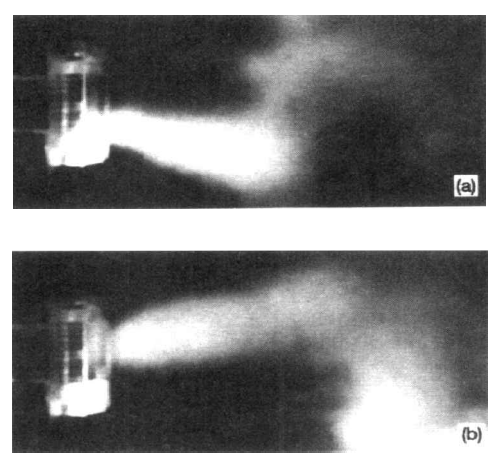

Fig. 3 Smoke flow visualization of oscillating flow produced by a fluidic excitation device. Panels a) and b) represent the two phases of oscillation.

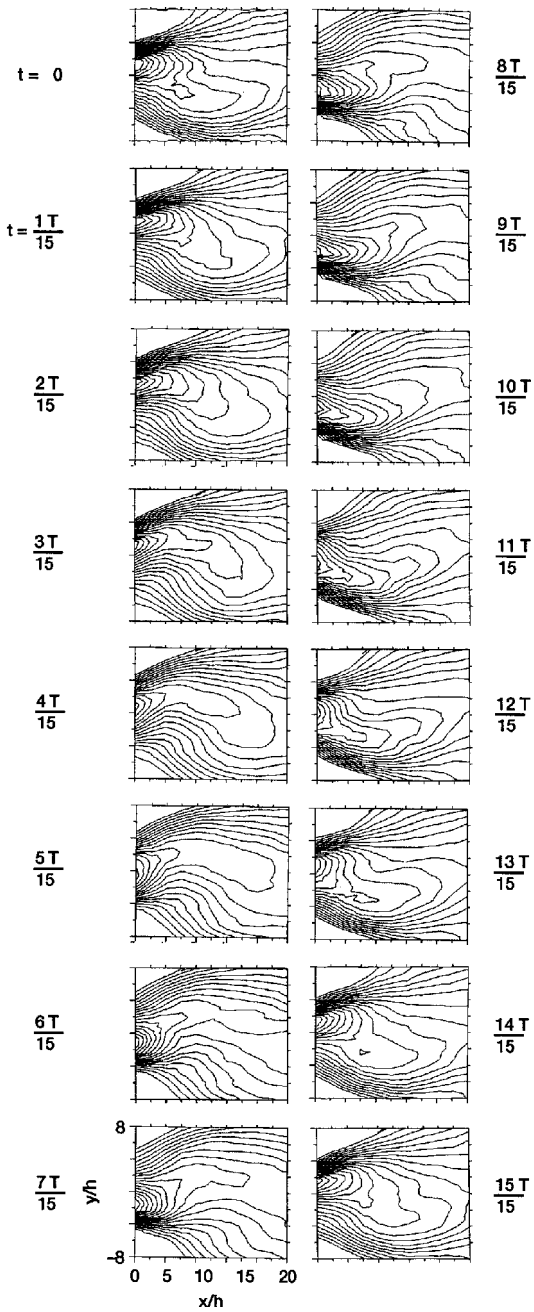

Fig. 4 Contours of $\langle u \rangle$ in the fluidic jet flowfield. The innermost and outermost contour levels are $\langle u \rangle / U_j$ = 1.0 and 0.4, respectively, with contour spacing $\langle u \rangle / U_j$ of 0.03.

time steps per oscillation period, only 16 are shown in Fig. 4, which clearly indicates the oscillatory nature of the flow. It can also be seen that the oscillating jet is indeed bistable (i.e., the jet spends more time at the walls and relatively less time transitioning from one wall to another). The frequency of oscillation scaled with h [$St(h)$] for the rectangular fluidic jet with an aspect ratio of eight.

For a rectangular fluidic jet with an aspect ratio of 8, the $St(h)$ is the appropriate nondimensional frequency. The $St(h)$ range over which the fluidic nozzle operated was 1 to 2 orders of magnitude below the $St(h)$ range of its natural flow instability. Rockwell[23] showed that the Strouhal number matching between the oscillation frequency and the natural flow instability was very important in determining the fate of the evolving flow. In the experiments of Vlasov and Ginevskiy,[24] excitation at $St_{\text{exc}} \gg St_{\text{natural}}$ resulted in turbulence suppression. Excitation at $St_{\text{exc}} \simeq St_{\text{natural}}$ resulted in mixing enhancement by the forced pairing of vortices.[25] Simmons et al.[26] showed that excitation at $St_{\text{exc}} \ll St_{\text{natural}}$ was equivalent to a periodic displacement of the entire jet shear layer.

In the fluidic jet in the present experiment, St_{exc} ranged from 0.001 to 0.01 and St_{natural} ranged from 0.1 to 0.6. Because $St_{\text{exc}} \ll St_{\text{natural}}$, the low-frequency oscillation of the entire jet produced a "pseudospreading" effect. For example, the ratio of the half-width of the fluidic jet to a rectangular nonoscillating jet $(y_{1/2})_{\text{fluidic}} / (y_{1/2})_{\text{rect}}$ was 1.21 at $x/h = 5$, 1.40 at $x/h = 10$, and 1.50 at $x/h = 15$. Thus, the half-velocity spread indicated that the fluidic jet spread by as much as 50% more than the rectangular jet at $x/h = 15$. The pseudospreading is confirmed by the mass flux ratio at any axial distance normalized by the initial mass flux ($\dot{m}/\dot{m}_o$). For the fluidic jet, $\dot{m}/\dot{m}_o$ at $x/h = 5$, 10, and 15 were 1.4, 1.95, and 2.50, respectively, whereas for the nonoscillating rectangular jet the corresponding values were 1.5, 1.85, and 2.50. Clearly, the differences in the mass flux ratio were small between the two cases being compared. Note that in addition to pseudospreading the fluidic jet is also affected by a shift in the virtual origin.

Thus, the low-frequency oscillation of the bistable fluidic jet results in pseudospreading—i.e., the time-mean spread is high, but, as seen from the phase-averaged realizations, the jet is at either one wall or the other. In addition, the fluidic nozzle produces an enormous thrust loss (20%). Consequently, the fluidic nozzle itself is not suitable for use as a primary jet nozzle when enhanced mixing is required. It can, however, be used as an excitation device to bring about "matched excitation" of a larger scale primary flow that has a lower natural instability frequency.

IV. Jet Excited by Unsteady Fluid Mass Addition

A. Arrangement of Fluidic Exciter Jets

The excitation configuration is shown in Fig. 5a. The fluidic jets (for clarity, somewhat exaggerated in size in the figure) were located $1.4 D_e$ away from the primary jet (on either side of the narrow dimension of the nozzle). The centerline of each exciter jet was oriented 30 deg to the centerline axis of the main jet. Air supply to each of the two fluidic jets, as well as the primary jet, was controlled independently. The operating conditions for the primary and fluidic jets are given in Table 1, and the xy and yz measurement planes are indicated in Fig. 5a.

The two fluidic exciter jets placed on either side of the narrow dimension of the rectangular jet oscillated in-phase to excite the sinuous mode in the primary jet. The fluidic nozzle interconnection scheme for producing sinuous and varicose modes is described in Ref. 17. Smoke flow visualizations of the unexcited and fluidically excited jets are shown in Figs. 5b and 5c, respectively. The photographs are single-exposure snapshots (0.0001 s) of the flow that freeze the flow. For the unexcited jet, some natural oscillations are visible farther downstream, whereas for the forced case a large-scale sinuous motion is clearly seen.

B. Frequency-Matched Unsteady Mass Addition Excitation

The importance of frequency matching between the excitation and the natural flow instability was discussed in Sec. III. Again, in exciting a primary jet using unsteady fluid mass addition, it is necessary to match the frequency of oscillation of the unsteady mass addition to the frequency range of the natural primary flow instability. The scaling parameter used was the Strouhal number based on the equivalent diameter of the rectangular nozzle (aspect ratio = 3). For rectangular jets of large aspect ratio ($\sim$10), the smaller dimension of the rectangular nozzle would have been the more appropriate length scale. Crow and Champagne[25] found the preferred jet column mode to be at $St(D_e)$ of 0.3. For the study reported here, the choice of forcing the subharmonic of the preferred jet column mode was made because its effect persists over a greater downstream distance.[27] Consequently, the frequency of oscillation of the fluidic jets was chosen to be 170 Hz, corresponding to $St(D_e)$ of 0.15.

For the primary rectangular jet flow, two fundamental modes of disturbance exist: sinuous and varicose. In such flows, it is the sinuous or coherent flapping oscillation of the entire jet[3] that is dominant farther downstream. Note that the large-scale antisymmetry produced by oscillation of the entire jet is different from a nonoscillating jet that has coherent structures that are symmetric about the centerline.[28]

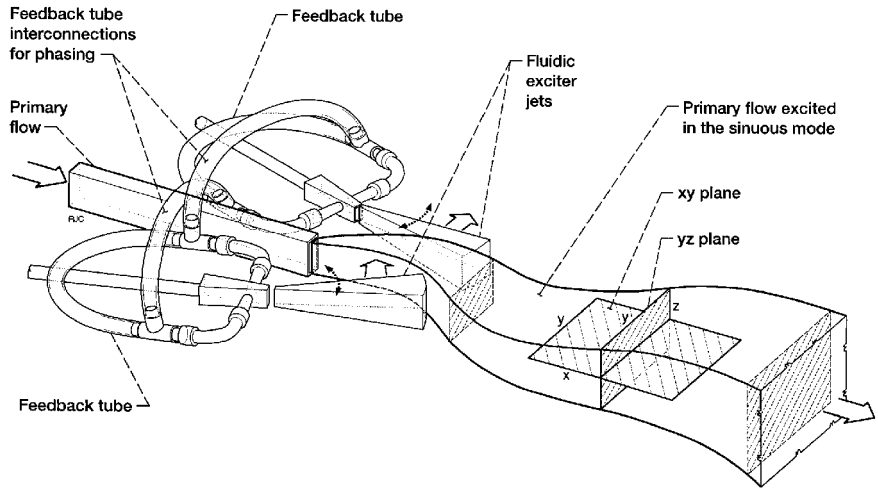

a) Arrangement of fluidic exciter jets on either side of the primary jet (fluidic jets are shown larger for clarity; actual dimensions are in Table 1)

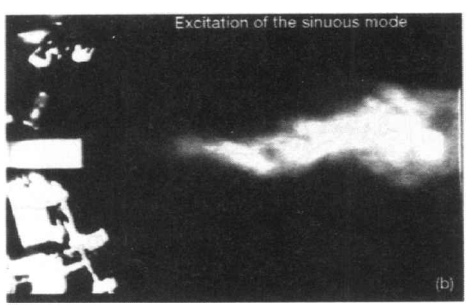

Smoke flow visualization of primary jet excited in the sinuous mode

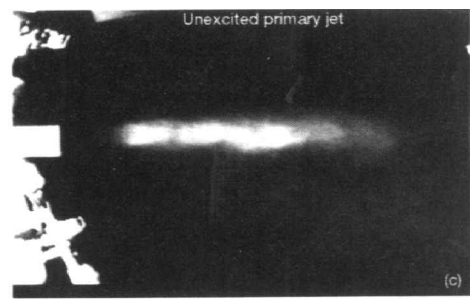

Smoke flow visualization of unexcited (natural) primary jet

Fig. 5 Schematic representation of unsteady fluid mass addition excitation.

C. Nozzle Exit Boundary Layer Documentation

In addition to the frequency and mode (sinuous) of forcing, the nozzle exit boundary layer is critical in determining the evolution of a jet.[29] To prevent the nozzle exit boundary layer from playing a role as a variable in this experiment, extra care was taken to ensure that the nozzle exit boundary layer state was the same for all cases being compared. The displacement and momentum thicknesses were obtained by integrating the nozzle exit boundary layer profiles. The integration was terminated at the 10% velocity point because measurements made with a hot wire may not be reliable near the outer edge of the jet. This choice of the integration limit, although having little effect on θ, results in an underestimation of δ^* and consequently of the shape factor. For the unforced primary jet, the δ^*/D_e, θ/D_e, and shape factor were 0.02827, 0.01807, and 1.56, respectively. For the primary jet forced in the sinuous mode, the corresponding values of δ^*, θ/D_e, and shape factor did not change very much and were 0.02728, 0.01815, and 1.503, respectively. Recall here that the shape factor for fully turbulent flow over a flat plate is 1.4. When the jet was excited in the sinuous mode, there was little effect on the state of the nozzle exit boundary layer.

D. Unsteady Features of the Fluidically Excited Jet

A reconstruction of the phase-locked flowfield of a jet excited by unsteady fluid mass addition is shown in Fig. 6. The phase averaging was performed with respect to a reference probe placed at the exit plane of one of the fluidic exciter jets. Although the phase-averaged distributions were computed for 40 time steps per period of oscillation, only 16 are reproduced in Fig. 6. The phase-averaged axial velocity component, $\langle u \rangle$, clearly shows the sinuous mode and its propagation downstream at phase speed $c = f\lambda = 2\pi f/\alpha_r$, determined to be $0.34\,U_j$. At this phase velocity, the sinuous disturbance is advected downstream over a distance of $4D_e$ within one period of oscillation. The effect of unsteady fluid mass addition on the phase-averaged velocity gradients and vorticity are shown in Fig. 7. The axial gradient, $(D_e/U_j)(\partial\langle v \rangle/\partial x)$, minus the transverse gradient, $(D_e/U_j)(\partial\langle u \rangle/\partial y)$, determined the vorticity. The two gradient terms are contributors to the phase-averaged strain rate and energy transfer from the phase-averaged flow to turbulence, respectively. Note that the phase-averaged measurements of $\langle u \rangle$ and $\langle v \rangle$ were performed over the entire xy plane and the derivatives obtained from these spatial measurements are more reliable than those obtained by the Taylor hypothesis $(\partial/\partial x_i) = -(1/U)(\partial/\partial t)$ in conjunction with a temporal measurement.

The $(D_e/U_j)(\partial\langle v \rangle/\partial x)$ gradients (Fig. 7a) display the high degree of organization produced by the fluidic excitation. However, the $(D_e/U_j)(\partial\langle v \rangle/\partial x)$ gradients are much smaller than the $(D_e/U_j)(\partial\langle v \rangle/\partial y)$ gradients shown in Fig. 7b. The resulting vorticity $(D_e/U_j)(\partial\langle v \rangle/\partial x) - (\partial\langle u \rangle/\partial y)$ is shown in Fig. 7c. It is clear from the data of Fig. 7 that the fluidic excitation persists over a considerable downstream distance. This point is confirmed by the spectra described in the following paragraph.

The evolution of spectra on the jet's centerline is shown in Fig. 8. The fluidic exciter jets, because of their on–off behavior, produced a quasi-square wave excitation waveform comprising a dominant frequency (f) and several harmonics (h denotes the first harmonic) (see Ref. 19). Beyond $x/D_e = 2$, the harmonics decayed, and only the primary fluidic excitation frequency persisted. Further, it was seen that the fluidic excitation introduced between $X/D_e = 0$ and 2 was barely perceptible on the centerline at the jet's exit but grew rapidly downstream and was sustained to x/D_e of 8. The low-frequency hump in the natural jet spectra indicates the range of frequencies to which the jet is unstable. The fluidic excitation and its harmonic are seen to match this unstable frequency range.

E. Features of the Resulting Mean Jet Flowfield

As mentioned in the Introduction, the motivation for this work was the expectation that controlled unsteady fluid mass addition at the correct frequency would enhance jet mixing significantly. It is therefore of interest here to document features of the mean flowfield resulting from this novel excitation method. Figure 9 shows detailed cross-sectional maps of the velocity field of the natural and fluidically excited jets. The left- and right-hand columns represent

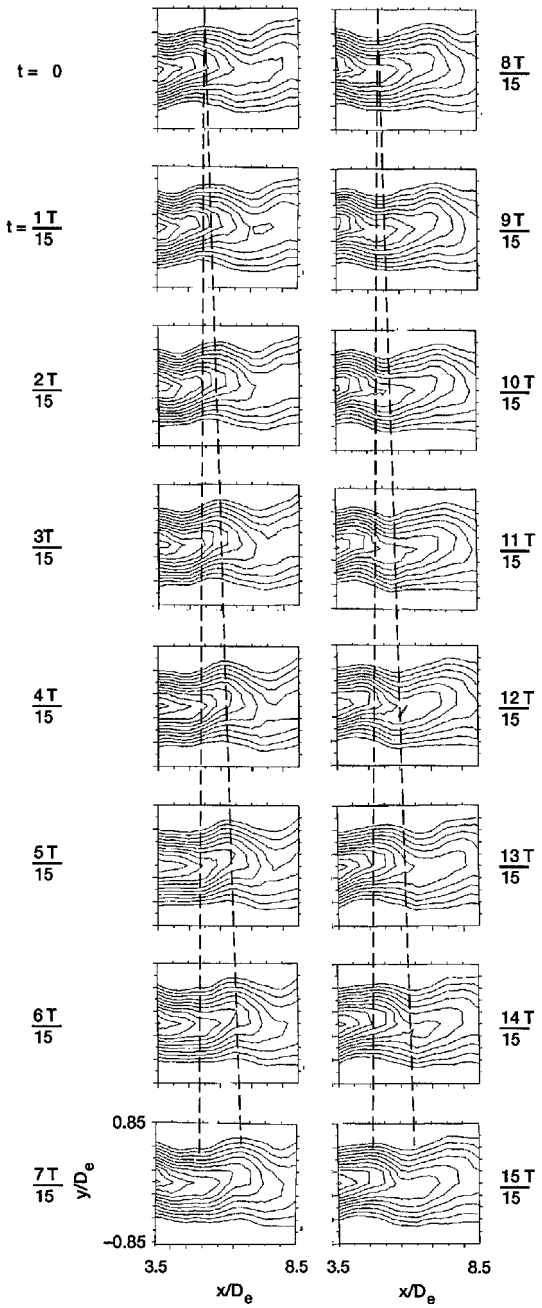

Fig. 6 Contours of $\langle u \rangle$ in the primary jet excited fluidically. The innermost and outermost contour levels are $\langle u \rangle / U_j$ = 1.0 and 0.5, respectively, with contour spacing $\langle u \rangle / U_j$ of 0.03.

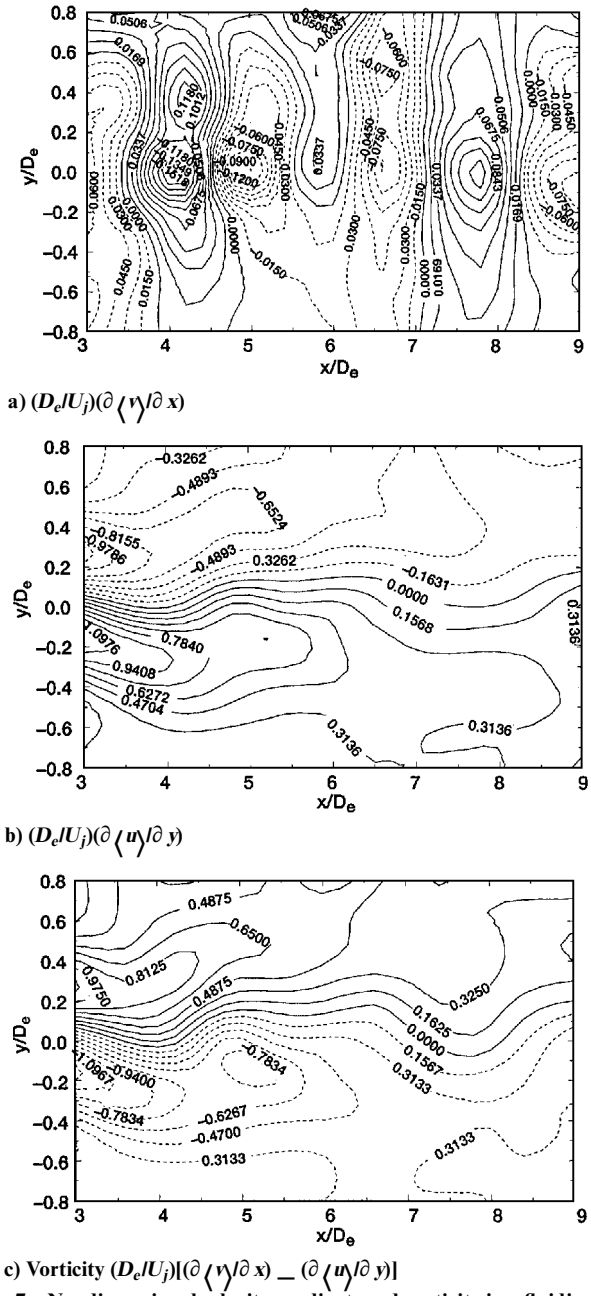

Fig. 7 Nondimensional velocity gradients and vorticity in a fluidically excited jet.

the natural (primary) and fluidically forced (primary + FF) cases, respectively. Figure 9 provides a pictorial view of the evolution of the mean flowfield for the two cases. For the forced jet cases, the magnitude and size of the fluidic jet flow as well as its interaction with the primary flow can be seen. For efficient operation of a fluidic excitation system, the mass flow through the exciter jets should be small compared to that through the primary nozzle. The mass flow through the primary nozzle was 0.0815 kg/s, whereas the mass flow through each of the fluidic jets was 0.0096 kg/s. Thus, the flow through each fluidic jet represented only 12% of the flow through the primary jet. It is observed that under excitation the jet spreads more rapidly and the velocity decays faster compared to the unforced case. Figure 10 shows the total streamwise velocity perturbation levels ($u\prime = \langle u_f \rangle + \hat{u}$) in a format similar to that in Fig. 9. The fluidic jets impart a very high $u\prime$ perturbation level to the primary jet in the initial region. The matched fluidic excitation level and the subsequent merging of the primary and the control jets produces a high $u\prime$ level spread over a larger region of the flow.

Figure 11a indicates a shorter potential core and a more rapid decay of the jet's centerline velocity for the forced than for the unforced case, which is in agreement with the data of Fig. 9. The data indicate a U/U_j value of 0.69 for the unforced case at x/D_e of 9. When the fluidic excitation was applied, the rectangular jet had an even faster centerline velocity decay ($U/U_j = 0.49$ at x/D_e of 9). The potential core length was shortened from $3D_e$ to $2D_e$ by application of fluidic excitation. The total streamwise velocity perturbation levels on the jet centerline are shown in Fig. 11b. The evolution of the turbulence in the jet has been moved upstream by the excitation. The turbulent fluctuations ($u\prime = \langle u_f \rangle + \hat{u}$) now peak at x/D_e of 1.8 compared to x/D_e of 3.25 for the unforced primary jet. Beyond x/D_e of 4, there is essentially no difference in the values of $u\prime$ on the jet's centerline between the forced and unforced cases.

For better quantification of jet mixing enhancement, the integral mass flux was calculated from the cross-sectional flowfield data of Fig. 9. The mass–flux ratio plotted on the ordinate of Fig. 12a is the ratio of the mass flux at any axial station to the initial mass flux. The initial mass flux is m_o for the unforced primary jet and $(m_o + 2m_{\mathrm{ffo}})$ for the forced case. It is clear that fluidic excitation produces very large changes in the entrained mass of the jet. Although the fluidic jet by itself does not entrain any more mass than the nonoscillating rectangular jet, matched fluidic excitation of a larger scale primary jet can have an enormous effect on the entrainment. The mass–flux

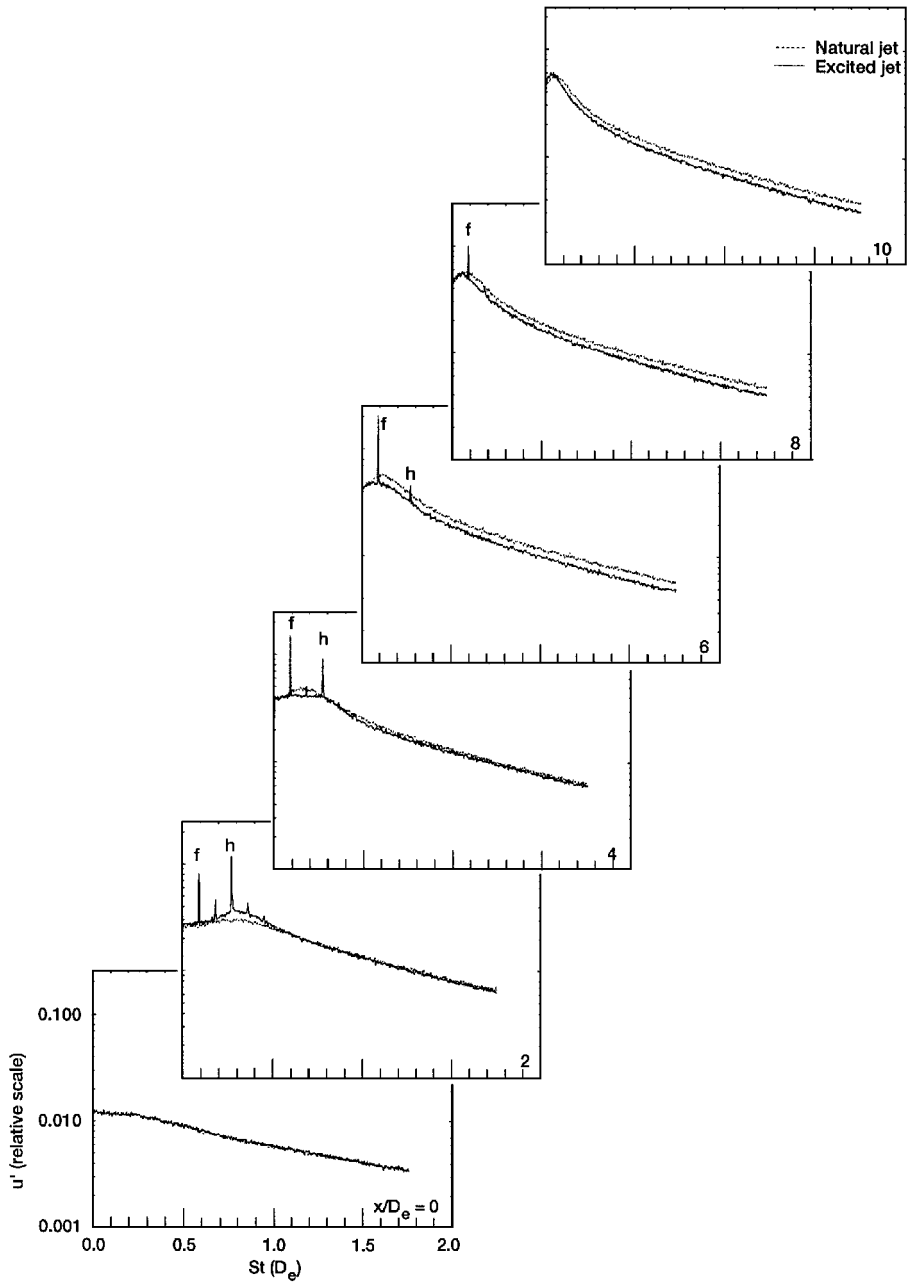

Fig. 8 Spectral evolution for the fluidically excited and natural jet cases (measured along the half-velocity point).

ratios of Fig. 12a show a higher slope for the excited case up to $x/D_e = 2$, beyond which the slopes are similar for the excited and natural jet cases. The net result is about a 60% increase in mass flux by $x/D_e = 3$.

A brief discussion comparing the present results with the two-dimensional jet results of Hussain and Thompson[2] and Thomas and Goldschmidt[30] and the rectangular jet results of Zaman[31] follows. Hussain and Thompson[2] used acoustic excitation with an amplitude equal to 1.4% of U_j over the $St(h)$ range from 0.15 to 0.6. The corresponding peak velocity fluctuations, at the excitation frequency $\langle u_f \rangle$, on the jet's centerline, range from 3 to 11% of U_j. In comparison, the value of $\langle u_f \rangle$ in the present work is 8% at $St(D_e)$ of 0.15. Hussain and Thompson[2] also reported a u/U_j peak of 0.2 in the shear layer in comparison to a value of 0.25 recorded in the present experiment. Hussain and Thompson's[2] normalized mean centerline velocities (U/U_j) were 0.94 at $x/h = 6$, 0.8 at $x/h = 10$, and 0.67 at $x/h = 15$. The present results give U/U_j values of 0.98 (unexcited) and 0.9 (excited) at $x/h = 6\,(x/D_e = 3)$, 0.86 (unexcited) and 0.69 (excited) at $x/h = 10\,(x/D_e = 5)$, and 0.67 (unexcited) and 0.5 (excited) at $x/h = 15\,(x/D_e = 7.5)$. Finally, the mass flux ratios (m/m_o) obtained by Hussain and Thompson[2] were 1.92 at $x/h = 6$, 2.6 at $x/h = 10$, and 3 at $x/h = 15$. The present work reports values of 1.4 (unexcited) and 2.35 (excited) at $x/h = 6\,(x/D_e = 3)$, 1.7 (unexcited) and 2.9 (excited) at $x/h = 10\,(x/D_e = 5)$, and 2.3 (unexcited) and 3.75 (excited) at $x/h = 15\,(x/D_e = 7.5)$.

Two points are to be noted from the Hussain and Thompson[2] data. First, their unexcited jet results indicate a higher jet decay and spread in comparison to the present unexcited jet results. Second, they did not observe significant changes in the spread when excitation was used. Both of these factors can be attributed to the presence of a laminar nozzle exit boundary layer in their experiments. Thomas and Goldschmidt[30] also did not observe any significant increase in jet spread with excitation up to $x/h = 20$ in their experiments. It is clear from the experiments performed by Lepicovsky and Brown[29] and from the data of Raman et al.[32] that jets with thin laminar nozzle exit boundary layers do not respond to excitation as do those with turbulent boundary layers. The present work uses a jet with a turbulent nozzle exit boundary layer, similar to the condition expected in full-scale jet engine exhaust.

Finally, the recent work of Zaman[31] shows that in low-aspect ratio rectangular jets acoustic excitation can be used to enhance jet mixing by inducing axis switching. A 50% increase in the jet's half-velocity spread at x/D_e of 7.5 was observed by Zaman. His results

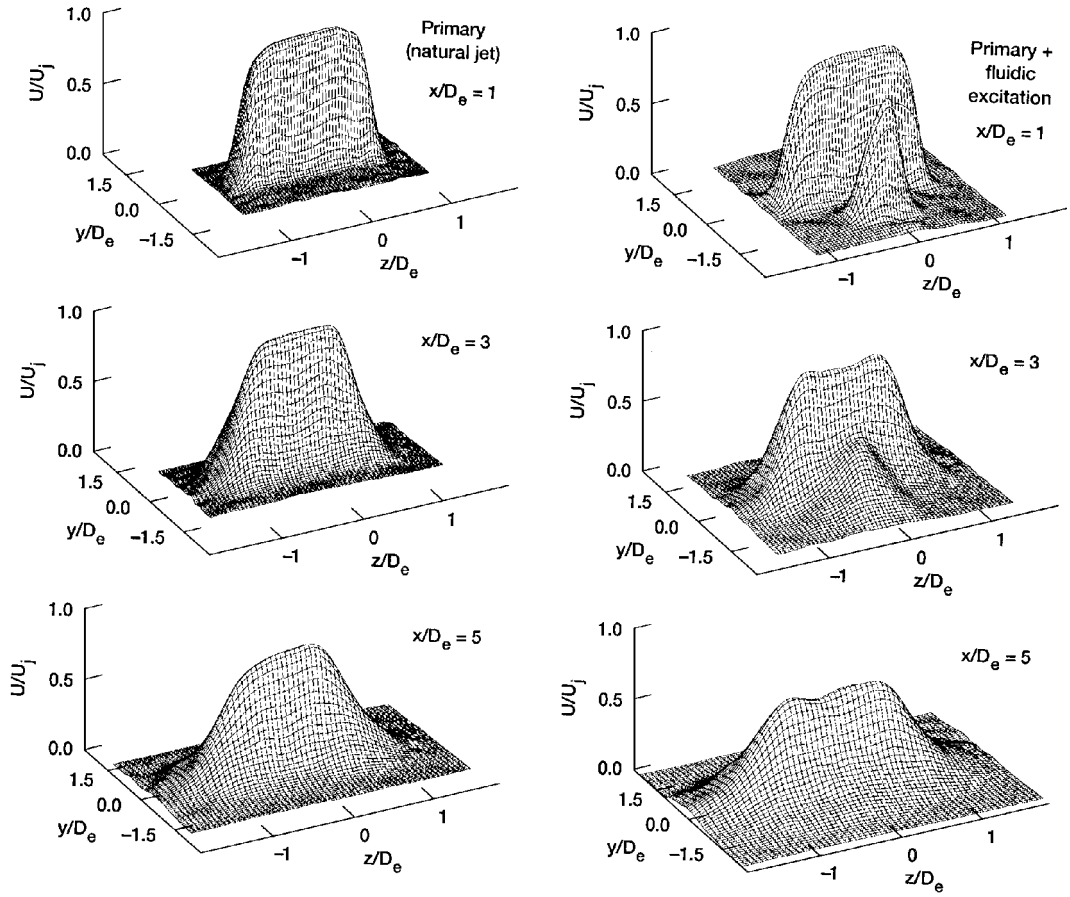

Fig. 9 Evolution of the mean velocity field for natural and fluidically excited jets.

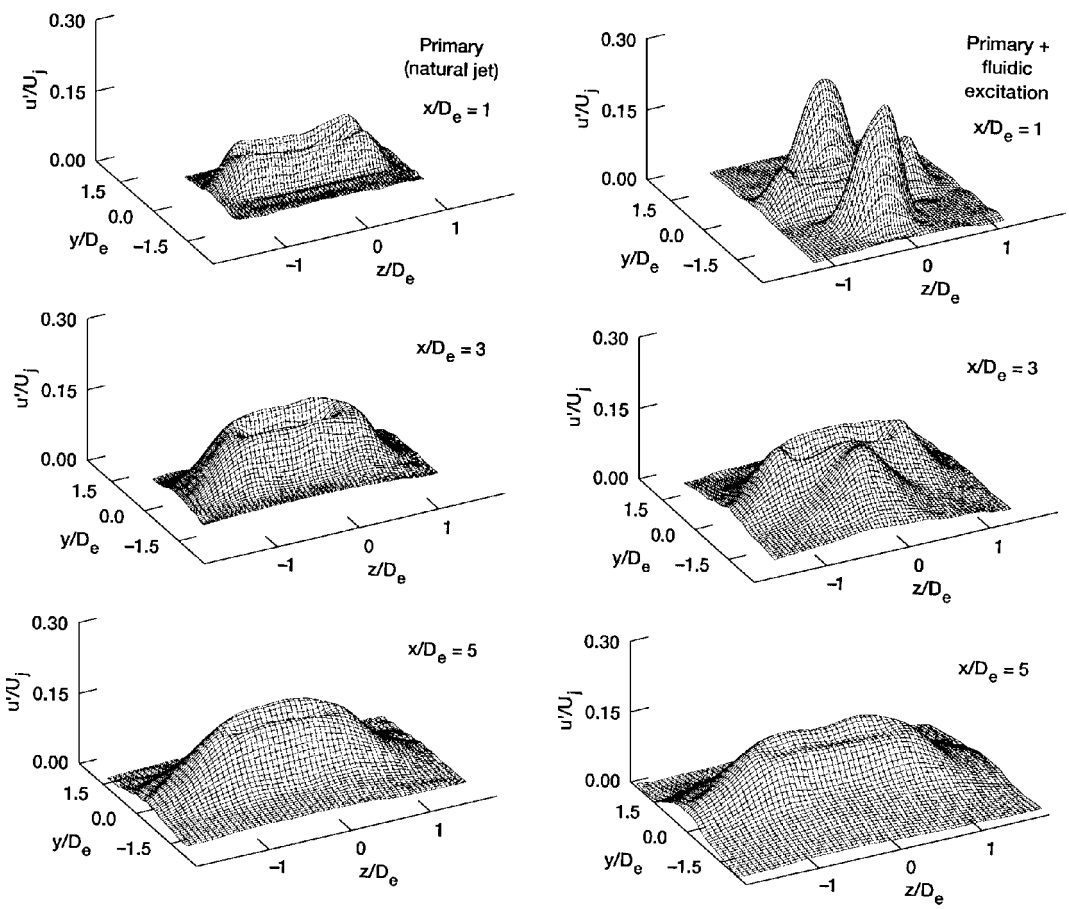

Fig. 10 Evolution of the streamwise velocity perturbation field [$u/U_j = (u + \langle u_f \rangle)/(U_j)$] for natural and fluidically excited jets.

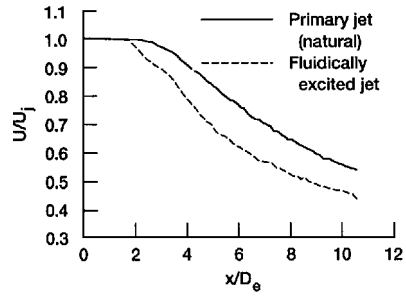

a) Jet centerline velocity

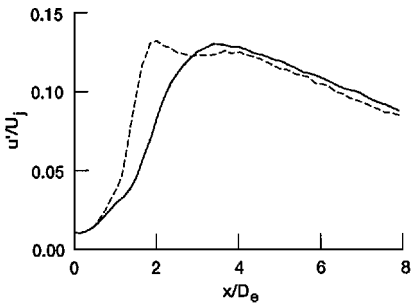

b) Jet centerline turbulence intensity

Fig. 11 Variation of mean and fluctuating velocities on the jet's centerline for natural and fluidically excited jets.

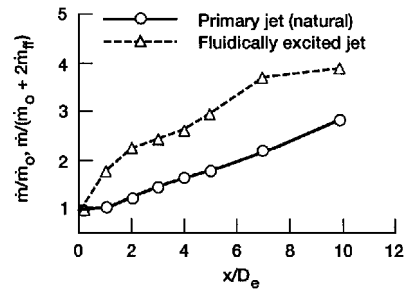

a) With downstream distance

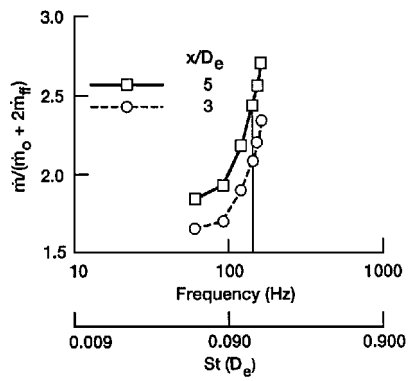

b) With frequency of excitation

Fig. 12 Variation of the integral mass–flux ratio.

are comparable to the 60% increase in mass flux and 35% reduction in the potential core length observed in the present experiment. However, note that there is no axis switch occurring in the initial region of the jet used in the present experiment.

One question remains: what is the effect of varying the frequency (recall that there are three harmonics) of the fluidic excitation? Because the fluidic exciter frequency depends on its operating nozzle pressure ratio, the mass addition also varies with frequency (see Fig. 2c). However, because the mass flux is normalized by $(m_o + 2m_{ffo})$ the effect of increased mass addition is factored out. The frequency effect is shown in Fig. 12b, where the frequency of fluid mass addition varied from 70 to 195 Hz [$St(D_e)$ from 0.063 to 0.172]. Again, note that at very low frequencies the entrained mass is not enhanced because of excitation, but as we near the natural flow instability range there is a significant increase in rate of increase of the mass flux.

There are two problems in going to higher frequencies. First, the mass flow through the exciter jets would also increase significantly, thus increasing the losses for this system. Second, the fluidic exciter cannot operate at very high frequencies. The present device can operate at 200 Hz. Frequencies up to 350 Hz can be obtained by shortening the feedback tube length or by increasing the feedback tube volume.[18] The first problem was solved in an earlier paper,[17] but the solution required two fluidic devices to operate in parallel with interconnected feedback tubes, with one device being the master and the second being the slave. In this manner, the frequency of the slave exciter could be controlled independent of mass flow. However, such a system proved too complex to use for the present experiment. Future work is required to improve the design and performance of such fluidic exciter devices.

V. Summary and Conclusions

A detailed exploration of a jet excited by unsteady fluid mass addition excitation was conducted. A pair of miniature fluidically oscillated jets that could produce a time-varying flow with a controllable frequency, magnitude, and relative phase (between the two oscillating jets) was used to excite a large-scale primary jet flow. The main motivation was provided by the expectation that unsteady fluid mass addition in the right frequency range would enhance mixing and thus provide a practical means to excite and control shear flow.

The primary jet was forced in the antisymmetric mode at the subharmonic of the primary's preferred jet column frequency [$St(D_e) = 0.15$]. However, because of the on–off (square wave) character of the exciter jets, harmonics at $St(D_e) = 0.3$, 0.45, and 0.6 were also excited. The primary jet had a turbulent nozzle exit condition, similar to the condition encountered in full-scale jet exhaust.

Details of the phase-averaged flowfield, velocity gradient terms, velocity spectra, and the mean and fluctuating flowfields were documented. The unsteady fluid mass addition excitation signal grew and persisted in the flow beyond the potential core region. The primary result was that fluid mass addition of 12% (4% momentum addition) per fluidic jet resulted in a 35% reduction of the potential core length and about a 60% increase in the normalized mass flux.

It is hoped that the fundamental experiments reported here will stimulate further study resulting in refinement of this technique and its use. The final technological goal is to develop and integrate multiple fluidic subelements into a system designed to solve an operational problem in a functioning complex device.

Acknowledgments

The author thanks J. Panda for providing a computer routine that was used for phase-averaged data acquisition. Thanks are also due to E. J. Rice for initiating the fluidic excitation work at NASA Lewis Research Center and to M. Hailye and D. Cornelius for their contributions to excitation device development (Refs. 16, 18, and 19) that made this work feasible.

References

[1] Ahuja, K. K., Lepicovsky, J., Tam, C. K. W., Morris, P. J., and Burrin, R. H., "Tone-Excited Jets, Theory and Experiments," NASA CR-3538, Nov. 1982.

[2] Hussain, A. K. M. F., and Thompson, C. A., "Controlled Symmetric Perturbation of the Plane Jet: An Experimental Study in the Initial Region," *Journal of Fluid Mechanics*, Vol. 100, No. 2, 1980, pp. 397–431.

[3] Cervantes de Gortari, J., and Goldschmidt, V. W., "The Apparent Flapping Motion of a Turbulent Plane Jet-Further Experimental Results," *Journal of Fluids Engineering*, Vol. 103, March 1981, pp. 119–126.

[4] Chambers, F. W., and Goldschmidt, V. W., "Acoustic Interaction with a Turbulent Plane Jet: Effects on Mean Flow," *AIAA Journal*, Vol. 20, No. 6, 1982, pp. 797–804.

[5] Parekh, D. E., Reynolds, W. C., and Mungal, M. G., "Bifurcation of Round Air Jets by Dual-Mode Acoustic Excitation," AIAA Paper 87-0164, Jan. 1987.

[6] Raman, G., and Rice, E. J., "Axisymmetric Jet Forced by Fundamental and Subharmonic Tones," *AIAA Journal*, Vol. 29, No. 7, 1991, pp. 1114–1122.

[7]Raman, G., Rice, E. J., and Reshotko, E., "Control of an Axisymmetric Turbulent Jet by Multi-Modal Excitation," *Proceedings of the Eighth Symposium on Turbulent Shear Flows* (Munich, Germany), 1991, pp. 6.2.1–6.2.6.

[8]Hill, W. G., and Greene, P. R., "Increased Turbulent Jet Mixing Rates Obtained by Self-Excited Acoustic Oscillations," *Journal of Fluids Engineering*, Vol. 99, June 1977, pp. 520–525.

[9]Strykowski, P. J., Krothapalli, A., and Jendoubi, S., "The Effect of Counterflow on the Development of Compressible Shear Layers," *Journal of Fluid Mechanics*, Vol. 308, Feb. 1996, pp. 63–96.

[10]Wiltse, J. M., and Glezer, A., "Manipulation of Free Shear Flows Using Piezoelectric Actuators," *Journal of Fluid Mechanics*, Vol. 249, April 1993, pp. 261–285.

[11]Parekh, D. E., Kibens, V., Glezer, A., Wiltse, J. M., and Smith, D. M., "Innovative Jet Flow Control: Mixing Enhancement Experiments," AIAA Paper 96-0308, Jan. 1996.

[12]Davis, M. R., "Variable Control of Jet Decay," *AIAA Journal*, Vol. 20, No. 5, 1982, pp. 606–609.

[13]Berman, C., and Andersen, O., "Auxiliary Jet Impingement to Reduce Jet Noise," AIAA Paper 96-0638, Jan. 1996.

[14]Viets, H., "Flip-Flop Jet Nozzle," *AIAA Journal*, Vol. 13, No. 10, 1975, pp. 1375–1379.

[15]Viets, H., "Coherent Structures in Time Dependent Shear Flows," NATO/AGARD CP 271, Sept. 1979, pp. 5.1–5.14.

[16]Raman, G., Hailye, M., and Rice, E. J., "Flip-Flop Jet Nozzle Extended to Supersonic Flows," *AIAA Journal*, Vol. 31, No. 6, 1993, pp. 1028–1035.

[17]Raman, G., and Rice, E. J., "Development of Phased Twin Flip-Flop Jets," *Journal of Vibration and Acoustics*, Vol. 116, July 1994, pp. 263–268.

[18]Raman, G., Rice, E. J., and Cornelius, D., "Evaluation of Flip-Flop Jet Nozzles for Use as Practical Excitation Devices," *Journal of Fluids Engineering*, Vol. 116, Sept. 1994, pp. 508–515.

[19]Raman, G., and Cornelius, D. M., "Jet Mixing Control Using Excitation from Miniature Oscillating Jets," *AIAA Journal*, Vol. 33, No. 2, 1995, pp. 365–368.

[20]Rice, E. J., and Zaman, K. B. M. Q., "Shear Flow Control by Artificial Excitation," AIAA Paper 87-2722, Oct. 1987.

[21]Brown, W. H., and Ahuja, K. K., "Jet Mixing Enhancement by Hydrodynamic Excitation," AIAA Paper 90-4005, Oct. 1990.

[22]Moffatt, R. J., "Using Uncertainty Analysis in the Planning of an Experiment," *Journal of Fluids Engineering*, Vol. 107, June 1985, pp. 173–178.

[23]Rockwell, D. O., "External Excitation of Planar Jets," *Journal of Applied Mechanics*, Vol. 39, April 1972, pp. 883–890.

[24]Vlasov, Y. V., and Ginevskiy, A. S., "Generation and Suppression of Turbulence in an Axisymmetric Turbulent Jet in the Presence of an Acoustic Influence," NASA TT-F-15721, June 1974, p. 721.

[25]Crow, S. C., and Champagne, F. H., "Orderly Structure in Jet Turbulence," *Journal of Fluid Mechanics*, Vol. 48, Aug. 1971, pp. 547–591.

[26]Simmons, J. M., Platzer, M. F., and Smith, T. C., "Velocity Measurements in an Oscillating Plane Jet Issuing into a Moving Stream," *Journal of Fluid Mechanics*, Vol. 84, Pt. 1, 1978, pp. 33–53.

[27]Merkine, L., and Liu, J. T. C., "On the Development of Noise Producing Large-Scale Wavelike Eddies in a Plane Turbulent Jet," *Journal of Fluid Mechanics*, Vol. 70, Pt. 2, 1975, pp. 353–368.

[28]Chambers, A. J., Antonia, R. A., and Browne, L. W. B., "Effect of Symmetry and Asymmetry of Turbulent Structures on the Interaction Region of a Plane Jet," *Experiments in Fluids*, Vol. 3, No. 6, 1985, pp. 343–348.

[29]Lepicovsky, J., and Brown, W. H., "Effects of Nozzle Exit Boundary Layer Conditions on Excitability of Heated Jets," *AIAA Journal*, Vol. 27, No. 6, 1989, pp. 712–718.

[30]Thomas, F. O., and Goldschmidt, V. W., "Acoustically Induced Enhancement of Widening and Fluctuation Intensity in a Two-Dimensional Turbulent Jet," *Journal of Fluids Engineering*, Vol. 108, Sept. 1986, pp. 331–337.

[31]Zaman, K. B. M. Q., "Axis Switching and Spreading of an Asymmetric Jet: the Role of Coherent Structure Dynamics," *Journal of Fluid Mechanics*, Vol. 316, June 1996, pp. 1–27.

[32]Raman, G., Zaman, K. B. M. Q., and Rice, E. J., "Initial Turbulence Effect on Jet Evolution With and Without Tonal Excitation," *Physics of Fluids*, Vol. 1, No. 7, 1989, pp. 1240–1248.

F. W. Chambers
Associate Editor